A preliminary study on intraparticle diffusion of turbidity through nanomagnetic biocarbon composite (NBC)

Palsan Sannasi Abdullah[1*], and *Huda* Awang[1]

[1]Faculty of Agro-Based Industry, Universiti Malaysia Kelantan Jeli Campus, 17600 Jeli, Kelantan, Malaysia

Abstract. The accessibility of safe drinking water is a fundamental element of Sustainable Development Goal 6 (SDG 6). A novel nanomagnetic biocarbon composite (NBC) has been developed utilising coconut shells for purifying raw groundwater. One of the primary concerns associated with groundwater is turbidity, a condition resulting from the presence of clay, dirt, and silt particles. The presence of turbidity in untreated water has a significant effect on both the visual appeal and overall cleanliness of the water. For the purposes of comparison, commercialised activated carbon (CAC) was utilised in this study. According to the Brunauer-Emmett-Teller (BET) analysis, it was observed that the average pore diameter of NBC was smaller compared to commercially available activated carbon (CAC), despite having a higher BET surface (SBET) value of 916.189 m/g compared to CAC. Based on the results of the kinetic study, it was determined that intraparticle diffusion, specifically external film diffusion, exhibited the most suitable fit as the kinetic model for NBC and CAC. This conclusion was supported by the lowest root mean square error (RMSE) values obtained, which were 0.04 for NBC and 0.13 for CAC, surpassing the performance of alternative models. The diffusion coefficient (Di) values for NBC (7.40 x 10–15 cm^2/s) and CAC (7.80 x 10–15 cm^2/s) demonstrated the phenomenon of bulk diffusion from high to low concentration. Notably, the diffusion coefficient for NBC was found to be lower than that for CAC. Accordingly, it is suggested that average pore diameter played important roles in intraparticle diffusion of an absorbent.

1 Introduction

Safe drinking water is essential for human sustainability and is considered a key aspect of the Sustainable Development Goals (SDGs) [1]. Over 70% of the water utilised for human consumption in Kelantan is sourced from groundwater. Although it is increasingly vital for drinking water, it is susceptible to contamination from excessive fertiliser use in agriculture, as well as seepage from sewers and landfills [2]. Individuals who consumed groundwater also encountered problems related to turbidity. The water's turbidity was caused by the

* Corresponding author:palsan.abdullah@umk.edu.my

presence of non-harmful particles, including clays, organic compounds, and soils. Ineffective purification leads to the formation of biofilms and oxide scales due to exposure to external contaminants, which poses a major obstacle to water filtration [3].

The turbid groundwater underwent various treatment processes, such as coagulation, flocculation, and adsorption, to achieve the desired level of purification and meet the drinking water standard of five NTU or less [4][5][6]. Harun et al. [5] found that copperas can be used as a coagulant to reduce turbidity in drinking water. However, the efficiency of copperas in removing turbidity is considered to be relatively low, ranging from 72.9% to 97.7%. Another study utilised proteolytic enzymes in together with alum for the treatment of highly turbid water. However, this approach was found to be expensive [6]. Many studies have utilised adsorption techniques, specifically employing materials like activated carbon and graphene oxide, to effectively remove turbidity [7]. At a concentration of 40 mg/L, the effectiveness of powdered activated carbon (PAC) in removing small amounts of turbidity was deemed insufficient. The turbidity reduction observed was 18.56% [8].

The study's findings recommend the use of biocarbon derived from agricultural waste as an adsorbent to remove turbidity from groundwater [9]. Agricultural waste were used as a suitable carbon source that could be easily modified through chemical and physical processes [10]. Pyrolysis involves the transformation of agricultural waste into biocarbon. The transformation took place under conditions of limited oxygen [7]. Typically, biocarbon material develops a stable mesoporous structure that is well-suited for adsorption processes [10]. Iron oxide nanoparticles were added to the biocarbon through chemical modification, as the nanoparticles are known for their magnetic properties. The effort aimed to enhance the efficiency of turbidity removal from groundwater [7]. Biocarbon's magnetic properties facilitated the separation of powdered adsorbent from an aqueous solution through the application of an external magnetic field [11].

The diffusion of reactant molecules into the adsorbent involved external film diffusivity, particle diffusion, and percent adsorption [9]. External film diffusivity refers to the movement of turbidity (adsorbate) from the fluid bulk onto the surface of NBC and CAC. Particle diffusion, on the other hand, involves the transport of adsorbate within the porous adsorbent. Percent adsorption is a measurement that quantifies the binding of adsorbate on the surface of NBC and CAC through a physical or chemical process [12]. This study specifically examined the relationship between the diameter of the solute molecule and the diameter of the adsorbent's pore. The primary challenge of this study is the presence of diverse molecule sizes in turbidity found in real samples. The primary objective of this study is to investigate the role of physical characteristics of NBC and CAC in intraparticle diffusion.

2 Materials and methods

2.1 Materials

The nanomagnetic biocarbon composite (NBC) was synthesised using coconut shell as the raw material. The procedures were conducted following the methodology outlined by Wannahari et al. [13]. The coconut shell was subjected to pyrolysis at temperatures ≥ 500°C in a top-lift updraft furnace for a duration of two to three hours, resulting in the production of powdered biocarbon. Subsequently, the powdered biocarbon underwent chemical precipitation using a solution containing 28% NH_3 in H_2O (ammonium hydroxide), iron (III) chloride hexahydrate ($FeCl_3.6H_2O$), iron (II) sulphate heptahydrate ($FeSO_4.7H_2O$), and epichlorohydrin (C_3H_5ClO). Subsequently, the precipitate underwent sonication at a temperature of 85°C for a duration of 1 hour using a Sonica Q device, followed by drying within a temperature range of 50-100°C. Subsequently, the dried NBC and powdered

commercialised activated carbon (CAC) were gathered, cleansed, and filtered using a sieve with a mesh size of < 45 µm. The materials will be used for further analysis.

2.2 Brunauer-Emmett-Teller (BET) and scanning electron microscopy (SEM) Analyses for Adsorbents.

The Brunauer Emmett Teller (BET) had been carried out for determination of surface area (m^2/g), average pore diameter (nm), total pore volume (cm^3/g), and pore size of NBC and CAC respectively. The analysis used a Quantachrome Autosorb iQ3 Automated Gas Sorption Analyzer with a nitrogen (N_2) adsorption desorption isotherm at 77K.

In addition to that, NBC and CAC were coated with aurum, later were subjected to scanning electron microscopy (SEM) (Model JSM IT-100, JOEL) (Magnification: 500 X; Accelerating voltage; 10-15 kV; Acquisition time: 40s).

2.3 Water sampling

Groundwater sample was collected from a well located in Tanah Merah, Kelantan (N 5 °4856.8 E 102 ˚ 0757.1).

2.4 Batch mode adsorption

The test was held with 10% adsorbent (NBC or CAC) in the working volume, and the condition of adsorbents were: 0.04 g of < 45 µm sized NBC and CAC ; Agitated at 150 rpm. The adsorbents were separated from liquid sample by using external magnetic field and filter paper. The turbidity of the sample was tested by using turbidity meter (Hanna Instrument) and the obtained data were used for plotting graphs. The turbidity removal efficiency was calculated as following equation:

$$Turbidity\ removal\ efficiency\ (\%) = \frac{Ti-Te}{Ti} \text{ x } 100 \quad (1)$$

Where, Ti and Te are denote for initial and final turbidity concentration (NTU) respectively.

The following equation was calculation for uptake capacity (q) of adsorbent:

$$q = \frac{(Ti-Te)v}{w} \quad (2)$$

Where, q is uptake capacity (mg/g), Ti and Te are initial and equilibrium turbidity (NTU) respectively, v is working volume (L) and w is weight of adsorbent (g).

2.5 Intraparticle diffusion kinetic models

Intraparticle diffusion (External film diffusivity) graph was plotted as qt against $t^{1/2}$.

$$qt = Kid\sqrt{t} + C \quad (3)$$

Based on the given equation, qt is the uptake capacity of adsorbate by adsorbent at time (mg/g), Kid is intraparticle diffusion rate constant (g/mg/min), c is an intercept value, and t is time (min) [14].

Furthermore, intraparticle diffusion (Particle diffusivity) was plotted for as ln (1-α) against t.

$$ln(1-\alpha) = Kidt \quad (4)$$

In this equation, α denotes for fractional attainment to equilibrium (qt/qe), t is time (min), and Kid is rate constant of intraparticle diffusion (NTU/min) [14].

In addition to that, the intraparticle diffusion (Percentage of adsorption) graphs was plotted as log R against log t.

$$log\, R = log\, Kid + a\, log(t) \quad (5)$$

In the given equation (equation 5), R is percentage of turbidity adsorbed at different times, t denotes as contact time (min), Kid is intraparticle diffusion rate constant (min^{-1}), and a denotes for adsorption mechanism [14].

Meanwhile, the diffusion rate constant was calculated as in equation 6:

$$Di = \frac{0.03r^2}{t0.5} \quad (6)$$

Where, Di is diffusion rate constant (cm^2/s), $t_{0.5}$ is time needed to complete half the adsorption (min), and r is radius of adsorbent (cm)\k [9].

The initial adsorption behavior was determined as following calculation:

$$qref = Kidt_{ref}^{0.5} + C \quad (7)$$

In this equation, $t_{ref}^{0.5}$ is longest time during adsorption process (min), qref is solid phase concentration, Kid is rate constant of intraparticle diffusion (NTU/min), and C is the value of intercept [9].

2.6 Intraparticle diffusion adsorption factor

The following equation shows calculation for initial adsorption factor:

$$Ri = 1 - (\frac{C}{qref}) \quad (8)$$

According to the given equation, Ri is ratio of the initial adsorption amount (c) to the final adsorption amount (qref), meanwhile, qref and C denote or solid phase concentration and value of intercept respectively [9].

Based on the given equation 8, initial adsorption behavior was determined according to table 1:

Table 1. Table for initial adsorption behavior, based on initial adsorption factor (Ri) and initial point of kinetic curve [9].

Initial Adsorption Factor (Ri)	Initial Point of Kinetic Curve (C/qref)	Initial Adsorption Behavior	Zone
Ri=1	C/qref =0	Not exist	0
1>Ri>0.9	0<C/qref<0.1	Weak	1
0.9>Ri>0.5	0.1<C/qref<0.5	Immediate	2
0.5>Ri>0.1	0.5<C/qref<0.9	Strong	3
Ri<0.1	C/qref>0.9	Approaching complete intial adsorption	4

2.7 Root mean square error (RMSE) calculation

The RMSE is important to measure accuracy between uptake capacity (q) of observation and predicted among three kinetic models of intraparticle diffusion. The calculation had been carried out as follows:

$$RMSE = \sqrt{\frac{1}{n}\sum_{i=1}^{n} Ri - Ei^2} \quad (9)$$

Where, Ri and Ei are reference and experimental values respectively as well as n is the number of observations recorded in analysis [15].

3 Results and discussions

Table 2 shows that NBC has a significantly higher BET surface area (S_{BET}: 916.20 m^2/g) compared to CAC (769.50 m^2/g). The average pore diameter of NBC is 14.60Å, significantly smaller than the average pore diameter of CAC, which measures 205.25Å. The findings demonstrate the presence of micropores, specifically those measuring less than 20 microns, on the surface of NBC. Moreover, the average pore diameter of CAC, which varies between 20 and 500 microns, indicates the existence of mesopores [16].

Table 2. Average pore diameter and BET surface area for NBC and CAC .

Types of Adsorbent	Average pore diameter (Å)	BET surface area (S_{BET}) (m^2/g)
NBC	14.60	916.20
CAC	205.25	769.50

Furthermore, Figure 1 illustrates the morphology of the NBC when observed under a magnification of 500x. The analysis reveals the existence of the NBC in the form of a dispersed assemblage of minute particles, each possessing a crystalline coating on its surface. In contrast, the morphology of the CAC, as depicted in Figure 2, exhibits the presence of pore formation on the adsorbent's surface. Consequently, this discovery is consistent with the findings presented in table 2.

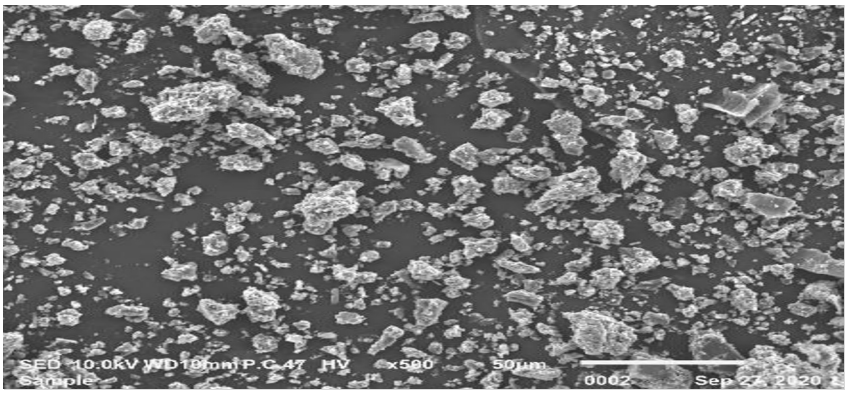

Fig. 1. Image of scanning electron microscopy (SEM) analysis for NBC at 500 X magnification.

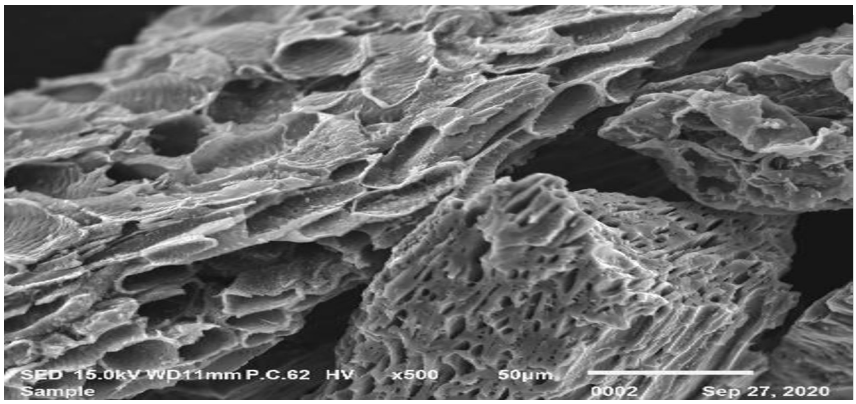

Fig. 2. Image of scanning electron microscopy (SEM) analysis for CAC at 500 X magnification

Figure 3 demonstrates that NBC is more effective at removing turbidity than CAC. Table 2 demonstrated that NBC had a higher S_{BET} than CAC. This is because a high S_{BET} will give a large surface area for groundwater turbidity absorption [17].

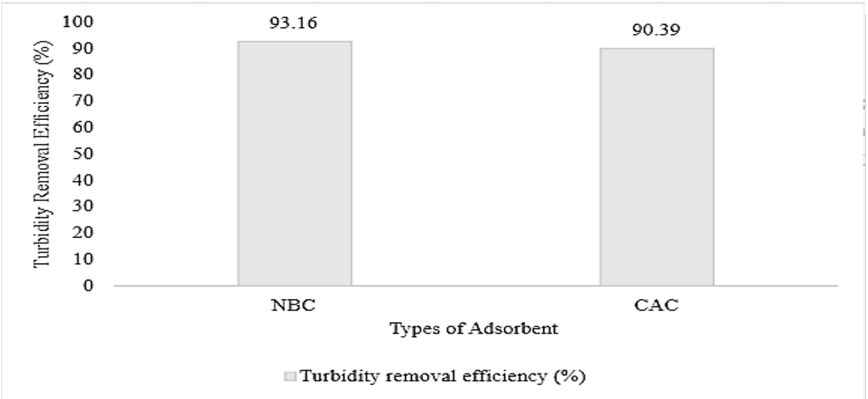

Fig. 3. Turbidity removal efficiency by NBC and CAC (0.04 g dosage, <45µm size of adsorbent, 150 rpm, and 60 min of rotation).

Figure 4-6 depicts turbidity intraparticle diffusion into the cavities of NBC and CAC particles. According to table 3, external film diffusion is the best fit intraparticle diffusion model due to the lowest RMSE; NBC (0.04) and CAC (0.13). These findings suggested that the turbidity intraparticle in groundwater is quite steep, and that it diffused into the adsorbent via the exterior aqueous film boundary layer (film diffusion) [18].

A comparison of plotted graph patterns (figure 4) for NBC and CAC revealed that the intraparticle diffusion of NBC is a straight line, indicating that it is a rapid diffusion and a non-rate limiting adsorption [19]. Meanwhile, figure 4 displayed a sigmoid curve shape, indicating that it is rate-limiting step diffusion, because instantaneous diffusion occurred between 1.73 and 4.8 minutes $^{1/2}$ and plateaued between 4.9 and 5.48 minutes ^{½} [19].

In addition, the intraparticle diffusion (external film diffusivity) constant (K_{id}) revealed the primary mechanism of diffusion [20]. Table 3 showed (K_{id}) was 0.3499 $gNTU^{-1}min^{-1}$ (NBC) and 0.9065 $gNTU^{-1}min^{-1}$ (CAC). CAC has a larger K_{id} value than NBC, indicating that its outer film diffusivity is more dominant. Betianu et al. [21] found that high

K_{id} values were associated with high initial turbidity concentrations and the well-known boundary layer effect. This conclusion was substantiated by the findings (table 3), which demonstrated that the boundary layer surrounding CAC was thicker than that surrounding NBC.

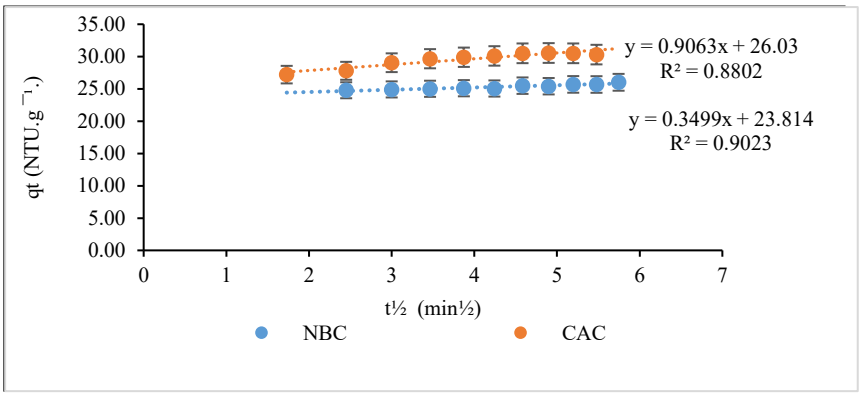

Fig. 4. Graph of intraparticle diffusivity (external film diffusivity) for turbidity removal from groundwater by using <45 µm of NBC and CAC.

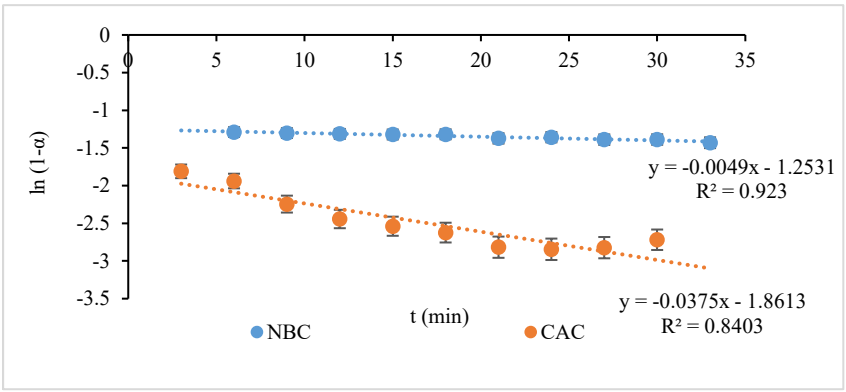

Fig. 5. Graph of intraparticle diffusivity (particle diffusion) for turbidity removal from groundwater by using <45 µm of NBC and CAC.

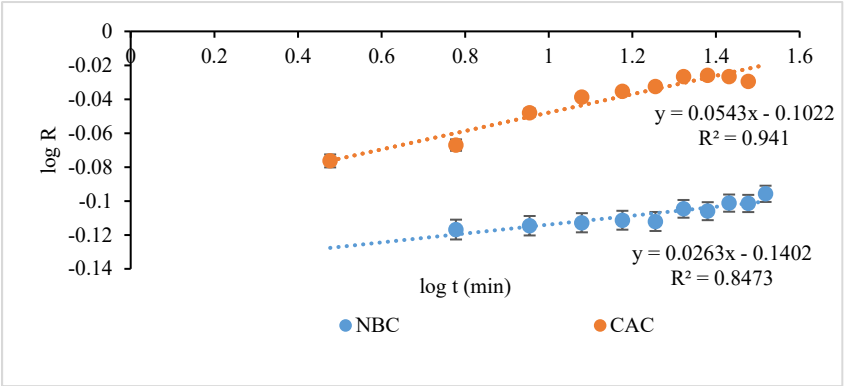

Fig. 6. Graph of intraparticle diffusivity (percent adsorption) for turbidity removal from groundwater by using 45 µm of NBC and CAC.

In addition, the diffusion coefficient (Di) for NBC (7.40 x 10^{-15} cm^2/s) and CAC (7.80 x 10^{-15} cm^2/s) is presented in table 3. Therefore, it is hypothesised that diffusion occurred when high turbidity in groundwater dispersed flux into a low concentration in a bulk [22]. In reality, the ratio of diffusing turbidity diameter to adsorbent pore diameter impacts the performance of the diffusion coefficient [23]. Table 1 shows that the average pore diameter of CAC is larger than that of NBC, indicating that larger pore diameters might attract more turbidity solutes to the pore wall.

Based on the data in Table 3, the combination of Ri (initial factor value) of 0.0778 and C/qref (ratio of initial adsorption to final amount of absorption) of 0.9221 indicates that NBC adsorption in zone 4 is nearing completion (Table 1). Table 3 shows that the values of Ri (CAC) and C/qref (CAC) are 0.1602 and 0.8398, respectively. These values fall within zone 3, indicating strong initial adsorption behaviour. The hypothesis suggests that the presence of iron oxide nanoparticles and a high specific surface area (SBET) of NBC (as shown in table 2) resulted in a significant surface area, which influenced the initial adsorption behaviour of NBC [9].

Table 3. Description of kinetic model and parameters for turbidity removal by NBC and CAC.

Kinetics Model		**Model Parameters**	**Types of Adsorbents**	
			NBC	CAC
Intraparticle Diffusion	External film diffusion	qe_{exp} (NTU g^{-1})	26.02	30.3
		qe_{ref} (NTU g^{-1})	25.8240	30.9941
		K_{id} (g NTU^{-1} min^{-1})	0.3499	0.9065
		Di (cm^2/s)	7.40 x 10^{-15}	7.80 x 10^{-15}
		C/qe_{ref}	0.9221	0.8398
		Ri	0.0778	0.160
		R^2	0.9023	0.8801
		RMSE	0.04	0.13
	Particle diffusivity	qe_{exp} (NTU g^{-1})	26.02	30.3
		qe_{calc} (NTU g^{-1})	-1.2531	-1.8613
		K_{id} (g. NTU^{-1} min^{-1})	-0.0049	-0.0375
		R^2	0.923	0.8403
		RMSE	8.24	9.23

	Percentage of adsorption	qe_{exp} (NTU g^{-1})	26.02	30.3
		qe_{calc} (NTU g^{-1})	-0.1402	-0.1022
		K_{id} (g NTU^{-1} min^{-1})	-0.1402	-0.1022
		R^2	0.8473	0.941
		RMSE	7.88	8.63

4 Conclusion

Consequently, it was determined that the intraparticle diffusion (external film diffusion) the best fit model for both NBC and CAC. In addition, NBC has higher S_{BET} and turbidity removal efficiency compared to CAC indicated the presence of iron oxide nanoparticles improved surface area and led to a high turbidity removal efficiency. Moreover, the intraparticle diffusion kinetics of NBC is a non- rate-limiting diffusion, in contrast to the intraparticle diffusion kinetics of CAC, which exhibited rate-limiting diffusion. Observations discovered that the average pore diameter of the adsorbent could influence the diffusion coefficient of turbidity from the groundwater sample to the pore wall of the adsorbent. This is implied by the observation that the average pore diameter influences the diffusion coefficient.

References

1. A.S. Asmadi, I.S. Saimy, N.A. Mohamed Yusof, S. Ba Qutayan S, S.H. Salleh 2023 *The Never-Ending Water Supply Scenario: A Case Study in Kelantan*, in Integrated Approaches to Peace and Sustainability (2023)
2. H. Shemeera, K. Prudhvi Raj, K. Prathyushac, *Analysis of groundwater quality and design of low-cost water purrifier* Int. J. Eng. Manag. Res **13** (2023)
3. WHO *Water quality and health-review of turbidity: Information for regulators and water suppliers Water Quality and Health-Review of Turbidity* (2017)
4. S.C. Chua, F. K. Chong, M.A. Malek, U.M. Muhammad Raza, I. Norli, W. Suwarjo, J.W. Lim, Y.C. Ho *Optimized use of ferric chloride and sesbania seed gum (SSG) as sustainable coagulant aid for turbidity reduction in drinking water treatment*, Sustain. **12** (2020)
5. M. Hakim, C. Harun, F. Fisol, S. Hamzah, F. Azaman*, Integration of iron coagulant, copperas , and calcium hydroxide for low-cost groundwater treatment in Kelantan, Malaysia,* Appl. NanoBioScience. **10** (2021)
6. B. Khaliq, H. Sarwar, A. Akrem, M. Azam, N. Ali, *Isolation of napin from Brassica nigra seeds and coagulation activity to turbid pond water* Water Supply. **22** (2022)
7. Q. Shi, W. Wang, H. Zhang, H. Bai, K. Liu, J. Zhang, Z. Li, *Porous biochar derived from walnut shell as an efficient adsorbent for tetracydine removal,* Bioresour. Technol. **383** (2023)
8. Q. He, L. Zhong, H. Wang, Z. Zou, D. Chen, K. Yang, *Odor removal by poedered activated carbon (PAC) in low turbidity drinking water,* Water Sci. Technol. Water Supply **16** (2016)
9. A. Pholosi, E.B. Naidoo, A.E. Ofomaja, *Intraparticle diffusion of Cr (VI) through biomass and magnetite coated biomass: A comparative kinetic and diffusion study, South African,* J. Chem. Eng. **32** (2019)

10. W. Long, Z. Chen, X. Chen, Z. Zhong, *Investigation of the adsorption process of chromium (VI) ions from petrochemical wastewater using nanomagnetic carbon materials*, *Nanomaterials* **12** (2022)
11. X. Song, Y. Zhang, N. Cao, D. Sun, Z. Zhang, Y. Wang, Y. We, Y. Yang, T. Lyu, *Sustainable chromium (VI) removal from contaminated groundwater using nano-magnetite-modified biochar via rapid microwave synthesis,* Molecules **26** (2021)
12. B. Obradovic*, Guidelines for general adsorption kinetics modelling*, Hem. Ind. **74** (2020)
13. R. Wannahari, P. Sannasi, M.F.M. Nordin, H. Mukhtar, *Sugarcane bagasse derived nano magnetic adsorbent composite (SCB-NMAC) for removal of Cu^{2+} from aqueous solution*, ARPN J. Eng. Appl. Sci. **13** (2018)
14.. C.Y. Abasi, A. A. Abia, J.C. Igwe, *Sorption kinetics and intraparticle diffusivities of Pb (II), Fe (II), and Cd (II) ions on unmodified Raphia palm fruit (Raphia hooker) endocarp,* Terr. Aquat. Environ. Toxicol. **6** (2012)
15. D.Christie P.S. Neill P S, *Ocean energy,* Comprehensive Renewable Energy (2022)
16. IUPAC, *Mesopore in catalysis,* Compendium of Chemical Terminology, 2nd ed. (the "Gold Book")(2019)
17. L. A. Barrera, A.C. Escobosa, A. Nevarez, M.A. Ahsan, L.S. Alsaihati, J.C. Noveron, *Nanoparticle-templated conversion of glucose to a high surface area biocarbon for the removal of organic pollutants in water,* Water Sci. Technol. **82** (2022)
18. J. Liu J, Y. Xu, *T-Friedman test: A new statistical test for multiple comparison with an adjustable conservativeness measure,* Int. J. Comput. Intell. Syst. **15** (2022)
19. M. Zbair, Z. Anfar, H. Ait Ahsaine, H. Khallok, *Kinetics, equilibrium, statistical surface modelling and cost analysis of paraquat removal from aqueous solution using carbonated jujube seed* RSC Adv. **9** pp 1084 (2019)
20. K.O. Yoro, M.K. Amosa, P.T. Sekoai, J. Mulopo, M.O. Daramola*, Diffusion mechanism and effect of mass transfer limitation during the adsorption of CO_2 by polyspartamide in a packed-bed unit*, Int. J. Sustain. Eng. **13** (2020)
21. C.S. Bețianu, P. Cozma, M. Roșca, E.D.C. Ungureanu, I. Mămăligă, M. Gavrilescu, *Sorption of organic pollutants onto soils: Surface diffusion mechanism of Congo red azo dye,* Processes **8** (2020)
22. M.V. Yarmolenko, *Method of dislocation and bulk diffusion parameters determination,s* Metallofiz. i Noveishie Tekhnologii **42** (2020)
23. E. Jacops, M. Aertsens, N. Maes, C. Bruggeman, R. Swennen, B. Kroos, A. Aman-Hildenbran, R. Littke R *The dependency of diffusion coefficients and geometric factor on the size of the diffusing molecule: Observation for different clay-based materials* Geofluids. **2017** (2017)